



available at www.sciencedirect.com



journal homepage: www.elsevier.com/locate/jhydrol



Development of a short-term river flood forecasting method for snowmelt driven floods based on wavelet and cross-wavelet analysis

Jan F. Adamowski *

MIT-Cyprus Institute Program, Massachusetts Institute of Technology, 77 Massachusetts Avenue,
02139-4307, Cambridge, MA, USA

Received 27 March 2007; received in revised form 29 January 2008; accepted 8 February 2008

KEYWORDS

Forecasting;
Wavelet transform;
Floods;
Time series

Summary In this study, a new method of stand-alone short-term spring snowmelt river flood forecasting was developed based on wavelet and cross-wavelet analysis. Wavelet and cross-wavelet analysis were used to decompose flow and meteorological time series data and to develop wavelet based constituent components which were then used to forecast floods 1, 2, and 6 days ahead. The newly developed wavelet forecasting method (WT) was compared to multiple linear regression analysis (MLR), autoregressive integrated moving average analysis (ARIMA), and artificial neural network analysis (ANN) for forecasting daily stream flows with lead-times equal to 1, 2, and 6 days. This comparison was done using data from the Rideau River watershed in Ontario, Canada. Numerical analysis was performed on daily maximum stream flow data from the Rideau River station and on meteorological data (rainfall, snowfall, and snow on ground) from the Ottawa Airport weather station. Data from 1970 to 1997 were used to train the models while data from 1998 to 2001 were used to test the models. The most significant finding of this research was that it was demonstrated that the proposed wavelet based forecasting method can be used with great accuracy as a stand-alone forecasting method for 1 and 2 days lead-time river flood forecasting, assuming that there are no significant trends in the amplitude for the same Julian day year-to-year, and that there is a relatively stable phase shift between the flow and meteorological time series. The best forecasting model for 1 day lead-time was a wavelet analysis model. In testing, it had the lowest RMSE value (13.8229), the highest R^2 value (0.9753), and the highest EI value (0.9744). The best forecasting model for 2 days lead-time was also a wavelet analysis model. In testing, it had the lowest RMSE value (31.7985), the highest R^2 value (0.8461), and the second highest EI value (0.8410). It was also shown that the proposed wavelet based forecasting method is not particularly

* Permanent address: 214 Goulburn Avenue, Ottawa, Canada, K1N 8E4. Tel./fax: +1 613 565 6146.
E-mail addresses: jfadamowskica@yahoo.ca, adamowsk@mit.edu

accurate for longer lead-time forecasting such as 6 days, with the ANN method providing more accurate results. The best forecasting model for 6 days lead-time was an ANN model, with the wavelet model not performing as well. In testing, the wavelet model had an RMSE of 57.6917, an R^2 of 0.4835, and an EI of 0.4366.

© 2008 Elsevier B.V. All rights reserved.

Introduction

Accurate flow forecasts are an integral component of sustainable water resources management systems. The importance of an accurate flow forecast, especially in flood prone areas, has increased significantly over the last few years as extreme events have become more frequent and more severe due to climate change and anthropogenic factors. The accuracy of models used for any flood forecasting and warning system is very important since an accurate flood forecast with sufficient lead-time can provide advanced warning of an impending flood at an early enough stage such that flood damages can be reduced significantly.

Data-based hydrological methods are becoming increasingly popular in flood forecasting applications due to their rapid development times, minimum information requirements, and ease of real-time implementation. Although they may lack the ability to provide physical interpretation and insight into catchment processes, they are nevertheless able to provide relatively accurate flood forecasts. In short-term flood forecasting applications where accuracy, reliability and robustness are required, data-based models are ideal.

In data-based flood forecasting, statistical models have traditionally been used. Multiple linear regression (MLR) and autoregressive moving average (ARMA) models are probably the most common methods for forecasting floods. More recently, artificial neural networks (ANN) have been introduced for flood forecasting applications. However, a problem with these and other linear and non-linear methods is that they have limitations with non-stationary data. In the last decade, wavelet analysis has been investigated in a number of disciplines outside of water resources engineering and hydrology, and it has been found to be very effective with non-stationary data. Wavelets are mathematical functions that give a time-scale representation of the time series and their relationships to analyze time series that contain non-stationarities. Wavelet analysis allows the use of long time intervals for low frequency information and shorter intervals for high frequency information and is capable of revealing aspects of data like trends, breakdown points, and discontinuities that other signal analysis techniques might miss. Another advantage of wavelet analysis is the flexible choice of the mother wavelet according to the characteristics of the investigated time series. To summarize, wavelet transforms provide useful decompositions of original time series, and the wavelet-transformed data improve the ability of a forecasting model by capturing useful information on various resolution levels.

Despite the above mentioned advantages, the use of wavelet analysis as a stand-alone flood forecasting method has not been explored in great detail in the literature, and this constituted the main purpose of this research.

Previous research

Regression, time series, and artificial neural network analysis

Many applications of regression methods can be found in the hydrological literature (Tangborn and Rasmussen, 1976; Curry and Bras, 1980; Phien et al., 1990; Tolland et al., 1998; among others). Examples of hydrological applications of ARMA and ARIMA models include McKerchar and Delleur (1974), Noakes et al. (1985) and Yurekli et al. (2005), among others. In one of the first applications of ANNs to river flow forecasting, Kang et al. (1993) used ANNs and ARMA models to predict daily and hourly river flows. They found that ANNs could be used for forecasting river flows. Since then, a number of studies have confirmed the usefulness of ANN models in river flow forecasting (among others, Hsu et al., 1995; Tawfik, 2003; Piotrowski et al., 2006). Kim and Barros (2001) used neural networks with radiosonde, rainfall data and satellite derived characteristics of storm systems for flood forecasting while Hsu et al. (2002) found that self-organizing linear output map neural networks provide features that facilitate insight into the underlying processes. And finally, Nayak et al. (2005) found that neurofuzzy models provided more accurate flood forecasts than neural network and fuzzy models.

Wavelet analysis

Wavelets, due to their attractive properties, have been explored for use in time series analysis. Examples in geophysics include the El Nino-Southern Oscillation (Gu and Philander, 1995), atmospheric cold fronts (Gamage and Blumen, 1993), and temperatures (Baliunas et al., 1997).

Wavelet transforms have become a tool for analyzing local variation in time series (Torrence and Compo, 1998), and hybrid models have been proposed for forecasting a time series based on a wavelet transform preprocessing (Aussem and Murtagh, 1997; Aussem et al., 1998; Zheng et al., 2000; Zhang and Dong, 2001). Wavelet transforms provide useful decompositions of original time series, so that wavelet-transformed data improve the ability of a forecasting model by capturing useful information on various resolution levels.

In the field of hydrology, wavelet analysis has been recently applied to examine the rainfall-runoff relationship in a Karstic watershed (Labat et al., 1999), and to characterize daily streamflow (Smith et al., 1998; Saco and Kumar, 2000) and monthly reservoir inflow (Coulibaly et al., 2000). It has been found that an appropriate data pre-processing stage using wavelet decomposition analysis can lead to models that more adequately represent the true features of the underlying system.

Several studies have been published that developed hybrid wavelet-ANN models. Wang and Lee (1998) developed a hybrid wavelet-ANN model to forecast rainfall–runoff in China, Kim and Valdes (2003) developed a similar model to forecast droughts in Mexico, and Cannas et al. (2005) developed a hybrid model for monthly rainfall–runoff forecasting in Italy. Each of these studies found that the ANNs trained with the pre-processed data had better performance than the ANNs trained with un-decomposed time series data, although the differences were small. As well, Tantane et al. (2005) developed a coupled wavelet-autoregressive model for annual rainfall prediction.

Outside of the hydrological and water resources literature, several authors have considered forecasting based on wavelet methods but not supplemented with neural networks. The forecasting method proposed by Wong et al. (2003) relies on the decomposition of the time series using wavelets into three summands: trend, harmonic and irregular components. The method of Soltani et al. (2000) exploits the de-correlating property of wavelets to forecast long-memory processes. Zheng et al. (2000) combine wavelets and Kalman filtering by modeling wavelet coefficients as state variables for the Kalman filter. Ikeda and Tokinaga (1999) use wavelets to forecast fractal time series.

There are a number of issues with respect to the use of wavelet analysis for flood forecasting within the areas of hydrology that have not, to the best knowledge of the author, been explored in detail in the literature:

1. The use of wavelet analysis as a stand-alone short-term river flood forecasting technique. The use of a stand-alone wavelet forecasting method based on daily forecasting models would permit the models to fully take advantage of one of the strengths of wavelet analysis (which is its ability to handle non-stationary data on a daily basis) because specific wavelet and cross wavelet derived daily values of amplitude, wavelength, phase and phase difference could be used in the forecasting models. Such a method was developed in this study.
2. The use of cross-wavelet analysis in the development of short-term river flood forecasting models. In this study, cross-wavelet analysis was used to determine the phase differences between flow and meteorological signals.
3. The use of wavelet decomposed meteorological data in addition to wavelet decomposed flow data for the development of models for short-term river flood forecasting. In order to be able to use the wavelet decomposed meteorological data for flood forecasting, a calibration constant has to be developed to link specific wavelengths of flow and meteorological cycles. Such a calibration constant was developed in this study.
4. The use of an edge effect correction technique developed from the continuous wavelet transform (CWT) for artificially split data. In order to account for edge effect discontinuities resulting from artificial data jumps, an edge effect correction technique was developed in this study.
5. The use of a modified version of the inverse Fourier transform with calibration constant and edge effect correction for short-term river flood forecasting. In order to

reconstruct wavelet decomposed signals, the inverse Fourier transform can be used. However, in order to allow for a more precise reconstruction, an edge effect correction and a calibration constant for meteorological signals was applied to the inverse Fourier transform in this study.

Study site and data

Rideau River watershed description

The Rideau River is located in southeastern Ontario, Canada, and flows northeast for approximately 110 km from its headwaters in the Lower Rideau Lake before discharging into the Ottawa River at Ottawa (shown in Fig. 1). The Rideau River watershed is a complex network of streams, rivers and lakes covering an area of about 3830 km². A flood forecasting and warning system for the Rideau River basin has been necessary to protect people from flood hazards and to reduce flood damages. The main reason for this is the annual snowmelt runoff flood, which is the most common type of flood in the Rideau River. This flood generally occurs in the spring in March and April each year. During this period of time, rapid melting of the snow under the combined effect of warmer temperatures, sunlight, and winds, releases significant quantities of water from the snow and the ice and causes a heavy runoff which raises the water levels in the Rideau River and causes flooding.

Rideau River data description

The data used in this study include a time series of stream flow of the Rideau River at the Ottawa station provided by the Rideau Valley Conservation Authority (RVCA), and a time series of meteorological data at the Ottawa International Airport obtained from Environment Canada for the Ottawa region (both locations are shown in Fig. 1). Only data from January to June were used in this analysis because the flood occurs in the spring months. The stream flow data consist of daily observations. The meteorological data consist of daily observations of maximum temperature, minimum temperature, rainfall, snowfall, and daily readings of snow pack depth on the ground. The temperature was taken 2 m above the ground. The meteorological variables were chosen since it was found that they were the most closely correlated with flow. For both the flow and meteorological data, the time series record begins in 1970 and ends in 2001. The data were divided into training and testing data sets. The former set began in 1970 and ended in 1997, while the testing set began in 1998 and ended in 2001.

Theoretical background

Wavelet transform

The Morlet–Grossman definition (Grossman and Morlet, 1984) of the continuous wavelet transform is

$$W(s, n) = \frac{1}{\sqrt{s}} \int_{-\infty}^{+\infty} x_{n'} \psi^* \left(\frac{n' - n}{s} \right) dn' \quad (1)$$



Figure 1 Rideau River watershed.

where $W(s, n)$ is the wavelet coefficient of the function $x_{n'}$, ψ is the analyzing wavelet (which is the Morlet wavelet in this study), $s (>0)$ is the scale, and n is the translation. Scale is the width of the wavelet: a larger scale means that more of the time series is included in the calculation and that finer details are ignored. A wavelet of varying width (scale) is moved or translated through the entire time series. The wavelet transformation is therefore localized in both time (through the translation) and frequency (through the range of scales).

There are a variety of wavelet functions that can be used. In this study, the complex non-orthogonal Morlet wavelet function was used, which can be used for signals with strong wave-like features (which is the case with streamflow data). The Morlet wavelet is a sinusoid with wavelength s modulated by a Gaussian function, and has provided robust results in analyses of time series records (Appenzeller et al., 1998; Gedalof and Smith, 2001). The parameter l is used to modify wavelet transform bandwidth-resolution either in favor of time or in favor of frequency, and represents the length of the mother wavelet or analysis window.

The shifted and scaled Morlet mother wavelet can be defined as (Morlet et al., 1982)

$$\psi_{s,n'}^l(n) = \pi^{-1/4} (sl)^{-1/2} e^{-i2\pi \frac{1}{s}(n-n')} e^{-\frac{1}{2}(\frac{n-n'}{sl})^2} \quad (2)$$

Cross-wavelet transform

When comparing two different variables like temperature or flow, or when analyzing tele-connections, one needs the bivariate extension of wavelet analysis. Cross-wavelet analysis was introduced, among others, by Hudgins et al. (1993). In hydrology, it has been used, for example, in rainfall-runoff cross analysis (Labat et al., 1999). In this research, cross-wavelet analysis was used to determine the phase difference $\Delta\phi_{n',s}$ values between the flow and meteorological variables, and to develop cross wavelet constituent components. The phase difference (shift) between variables x and y is defined by (Jury et al., 2002)

$$\Delta\phi_{x,y,n',s} = \tan^{-1} \frac{\int_{s1}^{s2} \text{Im}(W_{x,y,n',s}) ds}{\int_{s1}^{s2} \text{Re}(W_{x,y,n',s}) ds} \quad (3)$$

where Im and Re indicate the imaginary and real part, respectively. The cross-amplitude of variables x and y is defined by (Jury et al., 2002)

$$W_{x,y,n',s} = W_{x,n',s} W_{y,n',s} \quad (4)$$

Eq. (4) has the advantage that s is used unambiguously for both variables, resulting in very precise calibrations. For flow components, there is no $\Delta\phi_{n',s}$ term.

Model performance comparison

The performance of a model can be measured by the root mean square error (RMSE), the coefficient of determination (R^2), and the efficiency index (EI).

The root mean square error evaluates the variance of errors independently of the sample size, and is given by

$$RMSE = \sqrt{\frac{SEE}{N}} \quad (5)$$

where SEE is the sum of squared errors, and N is the number of data points used. SEE is given by

$$SEE = \sum_{i=1}^N (y_i - \hat{y}_i)^2 \quad (6)$$

where y_i is the observed flow, and \hat{y}_i is the computed flow from the model. The smaller the RMSE, the better the performance of the model.

The coefficient of determination (R^2) measures the degree of correlation among the observed and predicted values. It is a measure of the strength of the model in developing a relationship among input and output variables. The higher the R^2 value (with 1 being the maximum value), the better is the performance of the model. R^2 is given by

$$R^2 = \frac{\sum_{i=1}^N (\hat{y}_i - \bar{y}_i)}{\sum_{i=1}^N (y_i - \bar{y}_i)^2} \quad (7)$$

and

$$\bar{y}_i = \frac{1}{N} \sum_{i=1}^N y_i \quad (8)$$

where \bar{y}_i is the mean value taken over N , with the other variables having already been defined.

As a measure of accuracy, one can use the efficiency index (EI), which measures the agreement between simulated and actual values of a given parameter as a proportion of the total range of that parameter in the data. The value of the EI ranges from a maximum value of one to a minimum of minus infinity. The higher the value of the EI, the better is the performance of the model. It is given by (Nash and Sutcliffe, 1970)

$$EI = 1 - \frac{SE}{ST} \quad (9)$$

where SE is the sum square of errors given by

$$SE = \sum_{i=1}^N (y_i - \hat{y}_i)^2 \quad (10)$$

and ST is the total variation given by

$$ST = \sum_{i=1}^N (y_i - \bar{y})^2 \quad (11)$$

and

$$\bar{y} = \frac{1}{N} \sum_{i=1}^N y_i \quad (12)$$

where y_i is the observed value, \hat{y}_i is the forecasted value, and N is the number of data points.

Model development

Multiple linear regression, autoregressive integrated average, artificial neural network, and wavelet models were developed for 1, 2, and 6 days lead-time flood forecasting for the Rideau River in Ottawa, Canada.

Multiple linear regression analysis

Linear and multiple linear regression models were used to determine the relationship between stream flow for the current day F_t and the following variables: maximum temperature for the current day T_{max} , minimum temperature for the current day T_{min} , daily total rainfall for the current day R_t , daily total snowfall for the current day S_t , daily snow on the ground depth for the current day SG_t , daily snow on the ground depth for the previous day SG_{t-1} , and previous day stream flow F_{t-1} .

All of the MLR models were first trained (to determine the regression coefficients) using the data in the training set (1970–1997) and then tested using the testing data set (1998–2001), and compared using the three statistical measures of good fit. The S-Plus software package was used for regression calculations. Only the best regression model for each lead-time is provided in Table 1.

For 1 day lead-time forecasting, fifteen MLR models were developed. The best model, MLR (1)-1, is a function of daily stream flow from the previous day F_{t-1} , daily snow depth on the ground for the current day SG_t , daily snow depth on the ground for the previous day SG_{t-1} , daily total rainfall for the current day R_t , daily total snowfall for the current day S_t , maximum temperature for the current day T_{max} , and minimum temperature for the current day T_{min} . This model is given by

$$MLR(1)-1 = 3.401 + 0.96F_{t-1} - 0.775SG_t + 0.78SG_{t-1} + 0.50R_t + 0.12S_t - 0.33T_{max} + 0.34T_{min}$$

Table 1 Best multiple linear regression models for each lead-time

Model	Lead-time (day)	Equation
MLR (1)-1	1	$3.401 + 0.96F_{t-1} - 0.775SG_t + 0.78SG_{t-1} + 0.50R_t + 0.12S_t - 0.33T_{max} + 0.34T_{min}$
MLR (2)-1	2	$9.12 + 1.59F_t - 0.77F_{t-1} - 1.37SG_t + 1.55SG_{t-1} + 1.21R_t - 0.24S_t - 0.34T_{max} + 0.38T_{min}$
MLR (6)-1	6	$26.54 + 1.19F_t - 0.59F_{t-1} - 2.18SG_t + 2.47SG_{t-1} + 0.51R_t - 0.12S_t - 0.81T_{max} + 0.77T_{min}$

For 2 days lead-time forecasting, twenty MLR models were developed. Five more models were developed for 2 days lead-time compared to 1 day lead-time because more combinations of previous days were able to be used. The best model, MLR (2)-1, is a function of daily stream flow in the current day F_t , daily stream flow in the previous day, daily snow depth on the ground for the current day, daily snow depth on the ground for the previous day, daily total rainfall for the current day, daily total snowfall for the current day, maximum temperature for the current day, and minimum temperature for the current day. This model is given by

$$\text{MLR}(2)-1 = 9.12 + 1.59F_t - 0.77F_{t-1} - 1.37SG_t + 1.55SG_{t-1} \\ + 1.21R_t - 0.24S_t - 0.34T_{\max} + 0.38T_{\min}$$

For 6 days lead-time forecasting, twenty MLR models were developed. Five more models were developed for 6 days lead-time compared to 1 day lead-time because more combinations of previous days were able to be used. The best model, MLR (6)-1 is a function of daily stream flow in the current day, daily stream flow in the previous day, daily snow depth on the ground for the current day, daily snow depth on the ground for the previous day, daily total rainfall for the current day, daily total snowfall for the current day, maximum temperature for the current day, and minimum temperature for the current day. This model is given by

$$\text{MLR}(6)-1 = 26.54 + 1.19F_t - 0.59F_{t-1} - 2.18SG_t + 2.47SG_{t-1} \\ + 0.51R_t - 0.12S_t - 0.81T_{\max} + 0.77T_{\min}$$

Autoregressive integrated moving average time series analysis

There are four steps in model building: (a) testing for stationarity, (b) model identification (using ACF and other functions), (c) model verification (Akaike criterion or other tests), and (d) forecasting. Since the data were transformed into a stationary model through differencing, ARIMA models of order p , d , and q were used.

In the models that were developed, the number of autoregressive parameters (p) varied from 0 to 3 and the number of moving average parameters (q) varied from 0 to 3. One difference of the data set ($d = 1$) was required to transform the series into a stationary process. A total of twelve ARIMA models were selected to fit the trained stream flow series and the Akaike criterion (AIC) was used to verify each of the models. The best model for each lead-time is shown in Table 2 along with its coefficients and AIC value.

All of the ARIMA 'time series' models were first trained using the data in the training set (1970–1997) and then

tested using the testing data set (1998–2001), and compared using the three statistical measures of good fit. The S-Plus software program was used for all ARIMA calculations.

The best model for each lead-time is given by

$$\text{ARIMA}(1)-(3, 1, 0) = F_{t-1} + 0.6374(F_{t-1} - F_{t-2}) \\ - 0.1497(F_{t-2} - F_{t-3}) + 0.022(F_{t-3} - F_{t-4})$$

Artificial neural network analysis

Back propagation feed-forward ANNs with the 'generalized delta rule' (BP-MLP) as the training algorithm, were used to develop all the ANN models. The Tiberius 2.0.0 neural network modeling software package was used for the ANN analysis. To develop an ANN model, the primary objective is to arrive at the optimum architecture of the ANN that captures the relationship between the input and output variables. In this study, ANN networks consisting of an input layer with 1–8 input nodes, one single hidden layer composed of 4–7 nodes (1–8 were tested), and one output layer consisting of one node denoting the forecasted stream flow were developed. The optimum learning coefficients were found to be between 0.01 and 0.09 for the ANN models.

The inputs of each model consisted of all or some of the following variables: maximum temperature of the current day T_{\max} , minimum temperature of the current day T_{\min} , daily total rainfall for the current day R_t , daily total snowfall for the current day S_t , daily snow on the ground depth for the current day SG_t , daily snow on the ground depth for the previous day SG_{t-1} , the current daily stream flow F_t , and the previous daily stream flow F_{t-1} . Twenty-five models were developed for each lead-time. Only the best model for each lead-time is provided in Table 3. All of the ANN models were first trained using the data in the training set (1970–1997) to obtain the optimized set of connection strengths, and then tested using the testing data set (1998–2001), and compared using the three statistical measures of goodness of fit.

The best model for 1 day lead-time, ANN (1)-1, is a function of daily stream flow for the previous day, daily snow depth on the ground for the current day, daily snow depth on the ground for the previous day, daily total rainfall for the current day, daily total snowfall for the current day, and maximum temperature for the current day. This model had a 6–6–1 architecture and an optimized learning coefficient of 0.04.

The best model for 2 days lead-time, ANN (2)-4, is a function of daily stream flow for the current day, daily stream flow for the previous day, daily snow depth on the ground for the current day, daily snow depth on the ground for the previous day, daily total rainfall for the current day, daily total snowfall for the current day, and maximum temperature for the current day. This model had a 7–6–1 architecture and an optimized learning coefficient of 0.03.

The best model for 6 days lead-time, ANN (6)-1, is a function of daily stream flow for the current day, daily stream flow for the previous day, daily snow depth on the ground for the current day, daily snow depth on the ground for the previous day, daily total rainfall for the current day, daily total snowfall for the current day, and maximum

Table 2 Best autoregressive integrated moving average model for each lead-time

Model (p,d,q)	Equation	AIC
ARIMA (3,1,0)	$F_{t-1} + 0.6374(F_{t-1} - F_{t-2}) - 0.1497(F_{t-2} - F_{t-3}) + 0.022(F_{t-3} - F_{t-4})$	30543.52

Table 3 Best artificial neural network models for each lead-time

ANN model	Lead-time (day)	Network configuration I–H–O	Parameters	Learning coefficient
ANN (1)-1	1	6–6–1	$T_{\max}, R_t, S_t, SG_t, SG_{t-1}, F_{t-1}$	0.04
ANN (2)-4	2	7–6–1	$T_{\max}, R_t, S_t, SG_t, SG_{t-1}, F_t, F_{t-1}$	0.03
ANN (6)-1	6	7–6–1	$T_{\max}, R_t, S_t, SG_t, SG_{t-1}, F_t, F_{t-1}$	0.02

temperature for the current day. This model had a 7–6–1 architecture and an optimized learning coefficient of 0.02.

Proposed stand-alone wavelet flood forecasting method

The proposed stand-alone wavelet flood forecasting method is composed of the following steps:

1. *Data editing*: In order to reduce the number of variables in wavelet analysis, the variable 'precipitation' (P) was calculated using:

$$P = \text{Rain}(t) + \text{Snow}(t) + [\text{Snow on Ground}(t - 1) - \text{Snow on Ground}(t)] \quad (13)$$

Using the variable P (as opposed to R , S and SG as in the MLR, ARIMA, and ANN models) was necessary in the case of the wavelet models in order to reduce the number of possible model combinations because of the very high number of model combinations that could potentially be developed with the wavelet derived constituent components.

2. *Overview wavelet analysis*: Overview wavelet analysis was performed with a software program entitled CWTA.F (Prokoph and Barthelmes, 1996) in UNIX. In the overview wavelet analysis, the scales used ranged from 3 days to 5000 days and the translation (or shifting interval) was 5 days. Overview wavelet analysis was done on the flow (F), precipitation (P), minimum temperature (TI), and maximum temperature (TA) variables. The waveband subtitles for the wavelet analysis are shown in Table 4. The waveband subtitles 182, 48, 35, 25, 12, and 5 used in the forecasting models are simply 'designations' since the actual values (in addition to all other values) vary on a day to day basis from January 1st to June 30th.
3. *Cross-wavelet analysis*: Cross-wavelet analysis was performed with a software program entitled XCWT.F (Prokoph, 2006), which was very recently created as a companion software program for the CWTA.F software. Cross-wavelet analysis (XWA) was used to determine the phase difference values between the

flow and the meteorological variables once it was determined that a relatively stable phase shift existed between the flow and the meteorological variables.

4. *Calculation of histograms*: Histograms were created from the wavelength columns of the wavelet analysis results from the decomposition of flow, precipitation, and maximum and minimum temperature, in order to determine the frequency peaks, and to determine whether the same signals occur in the meteorological data as in the flow data so that the former can be used to effectively forecast the latter. In this manner, it was determined which wavelengths (periods) occurred most frequently and should therefore possibly be used in the construction of the forecasting models. The choice of signals was confirmed via spectral analysis.
5. *Spectral analysis*: Spectral analysis was used to confirm the results of the overview wavelet analysis and histograms in terms of the choice of major signals to be used in the reconstruction and forecasting models.
6. *Narrowband wavelet analysis*: Narrowband wavelet decomposition analysis was used to decompose the selected wavebands into their exact wavelengths with their amplitudes and phase. This step was done on the selected wavebands on all variables (i.e. F , P , TI, and TA). For narrowband wavelet analysis, the scales ranged from 3 days to 100 days (in order to make sure that the dominant 182 day waveband did not dominate). The translation used was 1 day.
7. *Calculation of edge effects*: Two types of edge effects influence the wavelet coefficients. The first edge effect is the decreased wavelet coefficients at the beginning and end of the data sets (1970 and 1997) due to the window width of the Morlet wavelet used. It does not play a strong role in the Rideau River case for two reasons. First, the use of $l = 5$ in this application results in the zero-padding 'overhang' not being very wide. And second, because the longest wavelength used (~ 182 days) is only about 3% of the entire record (~ 5075 days), only the beginning and end of the data sets (1970/1971 and 1996/1997) are influenced by edge effects. The shorter components are even less affected. As such, although the 'Morlet edge effect' is large for long wavelengths in other applications, it can be neglected in this application since all cycles are comparably small (smaller than 183 days). The second edge effect is the annual data cutoff on June 30th which provides un-natural signal jumps in all sub-annual cycles. This cutoff results in wavelet coefficients that are too high for the first and last days of each year. A correction technique was developed in this study to account for the annual data cutoff. For this correction, it was sufficient to use any single year

Table 4 Waveband subtitles for wavelet analysis

Waveband (days)	5–7	10–15	22–28	32–38	44–52	180–183
Waveband subtitle	5	12	25	35	48	182

(1972 was chosen) to correct for this jump since the jump was approximately the same amplitude each year. To account for the edge effects on the wavelet coefficients at the beginning and end of each year of artificially split data, an edge effect correction $Y_{n',s}$ was introduced (and is applied to data sets which have been artificially split). The edge effect correction in this case is defined by

$$Y_{n',s} = \frac{[W_{n',s}(\text{annual cycle of day} \times \text{for year } y)] / [W_{n',s}(\text{annual cycle average of day} \times \text{from beginning of cut data to end of cut data of year } y)]}{W_{n',s}(\text{annual cycle average of day} \times \text{for all training years})} \quad (14)$$

where n' is time, s is the waveband, $Y_{n',s}$ is the wavelet edge effect correction, and $W_{n',s}$ is the amplitude. As such, for each variable (i.e. F , P , TI , TA), a set of edge effect corrections for each day from January 1 to June 30 was calculated (having the same value for each year) and then applied to the 20–50 day cycles. Only the 20–50 day cycles were edge corrected because the annual cycle is shortened (i.e. 365–182 days) but not altered as the peak always appears approximately in the middle (i.e. approximately day 90–120) for each year. The short cycles (smaller than 20 days) are affected, but the last 10 and first 10 data points of each year were omitted for modeling and testing, thereby avoiding abrupt transitions (which would result in models that would likely be incorrect). This removal took care of the edge effects on the sub-20 day wavebands.

8. *Calculation of calibration constants:* A calibration constant was developed in this study which calibrates meteorological components to flow components. The calibration constant is the ratio in amplitude between each specific wavelength, and it permits forecasting of flow data by meteorological data by calibrating the meteorological components to the flow components of the same wavelength (e.g. temperature cycle to river flow cycle).

Calculation of calibration constants was done for the selected wavebands for P , TI , and TA . Each single day (i.e. 10593 days) of training data was used to calculate the calibration constants. The calibration constant $Z_{n',s}$ for each meteorological variable for each component was calculated by dividing the amplitude of the meteorological cycle from the corresponding amplitude of the flow cycle, and is shown by

$$Z_{n',s} = [W_{n',s}(\text{flow data})] / [W_{n',s}(\text{meteorological data})] \quad (15)$$

9. *Reconstruction of constitutive series:* From the above steps, the following was derived: (1) amplitude (i.e. wavelet coefficient) for each Julian day, for each component, for each variable (flow and meteorological); (2) wavelength for each Julian day, for each component, for each variable (flow and meteorological); (3) phase difference and phase for each component of each variable for each Julian day; (4) edge effect correction for each variable for each Julian day; and (5) calibration constant for each component of each mete-

orological variable. The average values of the above are shown in Tables 5–10. The wavelet constitutive components were reconstructed through the inverse Fourier transform multiplied by a calibration constant and an edge effect correction, along with a phase difference. For reconstruction, the wavelet coefficients (i.e. amplitude) were assumed to be equal to the Fourier amplitudes, and the Morlet wavelet scales were

assumed to be equal to the Fourier period. An assumption that was made was that there is a linear relationship between changes in amplitude of meteorological signals (e.g. temperature, precipitation cycles) and streamflow cycles, with particular calibration constants and differences in phase. Including the calibration constant, the phase difference between a meteorological component and its corresponding flow component, and noting that s defines the individual waveband (e.g. 40–45 days), while $s_{n'}$ defines the strongest wavelength inside the waveband s at location (or time) n' , each wavelet constitutive component was reconstructed for each Julian day by

$$x_{n',s} = Z_{n',s} Y_{n',s} W_{n',s} \left(\cos 2\pi \frac{n'}{s_{n'}} + \phi_{n',s} + \Delta \phi_{n',s} \right) \quad (16)$$

The parameters in the above equations vary through the year for each day, and as such explicitly take into account the daily non-stationarities in the data. In other words, there are separate constitutive series (and therefore forecasting models) for each specific day from January 1 to June 30 (the testing period the models were developed for). This is how the models should be used in an operational context. Only average values of the parameters are presented in the tables for the sake of succinctness.

10. *Calculation of averaged reconstructed constituent components:* The reconstructed daily constituent components were averaged for the same Julian day year-to-year for each day of the training period for the January 1 to June 30 period, and not the phase, amplitude, and wavelengths for each model. These averaged daily reconstructed components were then used in the construction of the forecasting models. This averaging assumed that there was no significant trend in the amplitudes, and that a relatively stable phase shift (i.e. phase difference) existed between F and the meteorological signals for the same Julian day year-to-year. This was the case for the Rideau River.
11. *Construction of forecasting models:* The best constructed wavelet forecasting models for each lead-time are shown in Table 11. An assumption that was made in the construction of the wavelet based models was that, in an operational context, one would have access to data for the flow $F(t)$ up to and including the $F(t)$ day. The actual forecasting models were con-

Table 5 Average amplitude for each wavelet component

	Average amplitude (m ³ /s)					
Waveband	5–7	10–15	22–28	32–38	44–52	180–183
Component	5	12	25	35	48	182
Flow (<i>F</i>)	7.401	15.223	23.601	25.312	31.943	52.082
<i>T</i> _{min} (TI)	3.054	3.283	3.353	3.253	3.492	11.452
<i>T</i> _{max} (TA)	2.817	3.117	3.231	3.070	3.364	12.642
Precipitation (<i>P</i>)	3.039	2.277	1.641	1.258	1.049	0.657

Table 6 Average wavelength for each wavelet component

	Average wavelength (days)					
Waveband	5–7	10–15	22–28	32–38	44–52	180–183
Component	5	12	25	35	48	182
Flow (<i>F</i>)	6.402	13.460	26.012	33.422	49.263	182.0
<i>T</i> _{min} (TI)	5.988	12.567	25.343	32.774	48.592	182.0
<i>T</i> _{max} (TA)	6.067	12.432	25.151	32.911	48.746	182.0
Precipitation (<i>P</i>)	5.756	11.992	24.404	32.648	47.095	182.0

Table 7 Phase difference for *F*(*t*) at *t* = 1 January 1st, 1970

	Phase difference					
Waveband	5–7	10–15	22–28	32–38	44–52	180–183
Component	5	12	25	35	48	182
<i>T</i> _{min} (TI)	1.82	1.61	–0.87	0.97	2.88	0.85
<i>T</i> _{max} (TA)	2.21	1.44	–1.24	1.08	2.9	0.93
Precipitation (<i>P</i>)	1.82	0.85	2.88	–1.93	–1.47	–1.43

Table 8 Phase for each wavelet component at *t* = 1 January 1st, 1970

	Phase					
Waveband	5–7	10–15	22–28	32–38	44–52	180–183
Component	5	12	25	35	48	182
Flow (<i>F</i>)	1.00	–1.06	3.12	–0.91	1.06	–2.62
<i>T</i> _{min} (TI)	3.10	3.00	1.72	2.53	–1.56	2.88
<i>T</i> _{max} (TA)	1.30	2.74	1.74	2.45	–1.58	2.79
Precipitation (<i>P</i>)	1.30	1.90	0.24	1.02	2.54	–1.19

Table 9 Average edge effect correction for each wavelet component

Component	Edge effect correction for long meteorological cycles
Flow (<i>F</i>)	1.00
<i>T</i> _{min} (TI)	1.38
<i>T</i> _{max} (TA)	1.30
Precipitation (<i>P</i>)	1.57

Table 10 Average calibration constants for wavelet components

Unit (days)	Calibration/attenuation constant		
	Precipitation (m ³ /s/mm)	<i>T</i> _{max} (m ³ /s/°C)	<i>T</i> _{min} (m ³ /s/°C)
182	70.1	6.3	6.9
45	70.3	19.6	22.8
32	85.7	20.1	25.2
22	30.2	20.3	20.3
10	5.1	3.3	2.8
5	2.3	2.6	2.2

Table 11 Constituent components for best wavelet models for each lead-time

Model	Lead-time (day)	Constituent components
Model (1)-M12	1	$F(t - 1) + T1182(t) - T1182(t - 1) + F48(t) - F48(t - 1) + TA12(t) - TA12(t - 1) + P5(t) - P5(t - 1) + F25(t) - F25(t - 1)$
Model (2)-M12	2	$F(t - 3) + T1182(t) - T1182(t - 3) + F48(t) - F48(t - 3) + TA12(t) - TA12(t - 3) + P5(t) - P5(t - 3) + F25(t) - F25(t - 3)$
Model (6)-M12	6	$F(t - 7) + T1182(t) - T1182(t - 7) + F48(t) - F48(t - 7) + TA12(t) - TA12(t - 7) + F25(t) - F25(t - 7) + P5(t) - P5(t - 7)$

structured from the flow data of the previous day (or 3 days ago or 7 days ago) plus the difference between the current day output from a constitutive series- y and the previous day (or 3 days ago or 7 days ago) output from the same constitutive series- y (or more cycles). In order to obtain the best possible overall wavelet model, stepwise correlation was used for optimization. The best wavelet model was constructed by assessing the correlation (R^2) of each component with the training $F(t)$, and taking the best correlating components as the basis and adding the other components successively to the model depending on whether the forecast improved or not. For 1 day lead-time, the best overall wavelet model, WT(1)-M12 (M = mixed),

$$F(t - 1) + [T1182(t) - T1182(t - 1)] \\ + [F48(t) - F48(t - 1)] + [TA12(t) - TA12(t - 1)] \\ + [P5(t) - P5(t - 1)] + [F25(t) - F25(t - 1)]$$

where F = flow, TI = minimum temperature, TA = maximum temperature, and P = precipitation. This model was developed based on the flow from the day before and the difference between the current day output from each constitutive cycle of a variety of components, and the previous day output from each constitutive cycle of a variety of components. For 2 days lead-time, the best overall wavelet model, WT (2)-M12, can be written as

$$F(t - 3) + [T1182(t) - T1182(t - 3)] \\ + [F48(t) - F48(t - 3)] + [TA12(t) - TA12(t - 3)] \\ + [P5(t) - P5(t - 3)] + [F25(t) - F25(t - 3)]$$

This model was developed based on the flow from three days before and the difference between the current day output from each constitutive cycle of a variety of components, and the output from three days before of each constitutive cycle of a variety of components. For 6 days lead-time, the best overall wavelet model, WT (6)-M12, can be written as

$$F(t - 7) + [T1182(t) - T1182(t - 7)] \\ + [F48(t) - F48(t - 7)] + [TA12(t) - TA12(t - 7)] \\ + [P5(t) - P5(t - 7)] + [F25(t) - F25(t - 7)]$$

This model was developed based on the flow from seven days before and the difference between the current day output from each constitutive cycle of a variety of components, and the output from seven

days before of each constitutive cycle of a variety of components. In an operational context, the above models would be used with the component parameter values from the specific day to be forecasted and component parameter values from the current day needed to forecast the flow for that specific day. As well, the flow value for the current day would be used. For example, in the case of 1 day lead-time, model WT (1)-M12 would be used as follows in an operational context

$$F(t + 1) = F(t) + [T1182(t + 1) - T1182(t)] \\ + [F48(t + 1) - F48(t)] + [TA12(t + 1) \\ - TA12(t)] + [P5(t + 1) - P5(t)] \\ + [F25(t + 1) - F25(t)]$$

where the only 'external' value needed is the $F(t)$ value which would be obtained from the flow station for that current day, and with all other values having already been calculated for that specific day in the development of the forecasting models.

12. *Testing of constructed forecasting models:* As with the MLR, ARIMA, and ANN models, the wavelet (WT) models were tested on data from 1998 to 2001 by comparing the original $F(t)$ or observed flow with the forecasted output of the models. Models were compared using the coefficient of determination (R^2), the efficiency index (EI), and the root mean square error (RMSE). As well, a simple perseverance model for flow was tested for comparative purposes.

Results

Overview wavelet analysis

The shortest recognizable signals occurred in the 5–6 day spectrum and the longest in the 180–183 day spectrum. No significant multiyear signals were found. In total, six major wavebands were identified, and were later confirmed through the use of histograms and power spectra: a dominant and stationary 182 day cycle (i.e. annual cycle for these data), and weaker, non-stationary cycles of approximately 5, 12, 25, 35, and 48 days.

Overview wavelet scalograms and phase spectrum figures

From the overview wavelet scalogram of the F data in Fig. 2 one can see the strength of the six major wavebands (i.e.

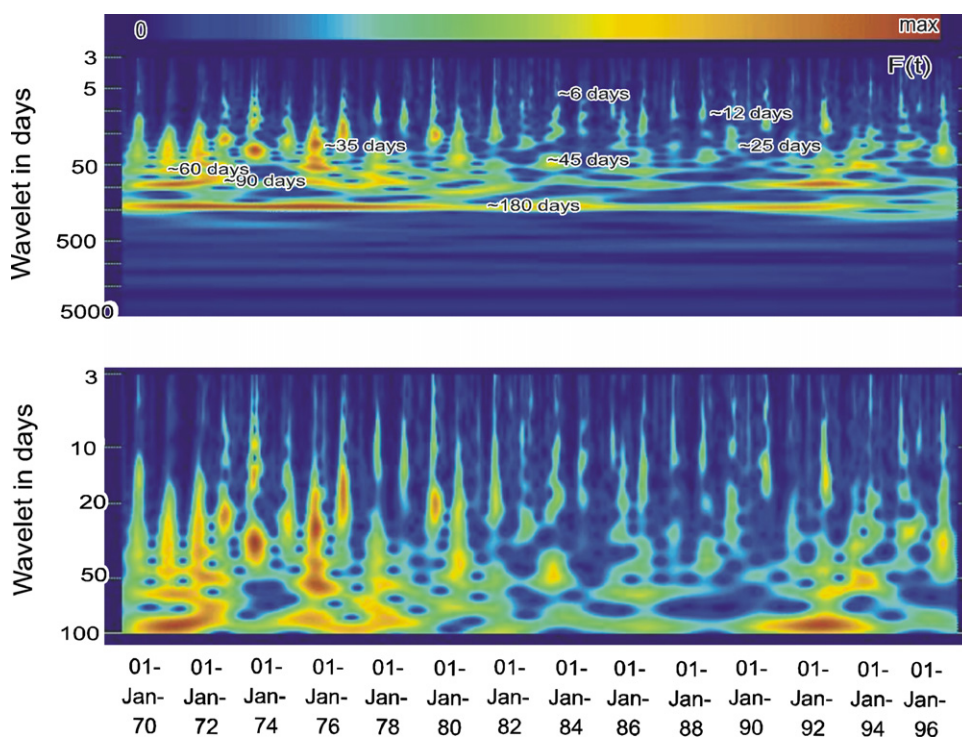


Figure 2 Overview and narrowband wavelet analysis of Rideau River flow-training data top = overview analysis and bottom = narrowband analysis.

~6 days, ~12 days, ~25 days, ~35 days, ~45 days, and ~180 days). Horizontal lines indicate stationarity while 'speckled' data indicate non-stationarity. The long horizontal yellow/orange line around the 180 day scale in the scalogram indicates that the annual signal is stationary.

From the overview wavelet scalogram of the TI and TA data in Fig. 3, one can see the presence of the six major wavebands (i.e. ~6 days, ~12 days, ~25 days, ~35 days, ~45 days, and ~180 days). As with the flow data, the long horizontal yellow/orange line around the 180 day scale in the scalogram indicates that the annual TI and TA signals are stationary.

From the overview wavelet scalogram of the P data in Fig. 3, one can see that the precipitation pattern is dominated to a much larger extent by non-stationary short wavelengths (high frequencies) than the flow data. Non-stationarity can be observed here as the fluctuation between dark and light blue. The lighter blue vertical lines indicate the June–January discontinuities.

Cross-wavelet analysis

Cross-wavelet analysis was used to determine the specific phase difference values between flow and meteorological variables. The phase difference values at $t = 1$ (i.e. January 1st, 1970) can be found in Table 7.

Cross-wavelet scalogram and phase difference spectrum figures

From the cross-wavelet scalograms (the top figures) of the logarithmically spaced flow data with the precipitation,

minimum temperature, and maximum temperature data shown in Fig. 4, one can see the dominance of the stationary 182 day cycle (the horizontal yellow/orange¹ band). Yellow/orange indicates maximum cross-amplitude and a horizontal line indicates stationarity. As such, the horizontal yellow/orange band of the 182 day cycle visually demonstrates the dominant and stationary 182 day cycle.

Histograms

The histograms of the frequency of signal occurrences from the wavelet analysis of the flow data indicated that strong peaks occur at approximately 180 days, 48 days, 33 days, 20–28 days, 10–14 days, and approximately 5 days. For the meteorological data, it was found that strong peaks occur at ~180 days (TI, TA, P), ~48 days (TI, TA), 33 days (TI, TA), 20–28 days (TI, P), 10–14 days (P), and ~5 days (P).

Power spectra

Power spectra via Fourier analysis was used to confirm the results of the overview wavelet analysis and histograms in terms of the choice of major signals to be used in the reconstruction and forecasting models. The power spectra confirmed the results of the overview wavelet analysis and histograms in terms of the choice of the six major wavebands (i.e. approximately 5, 12, 25, 35, 48 and 182 day cycles).

¹ For interpretation of color in Fig. 4, the reader is referred to the web version of this article.

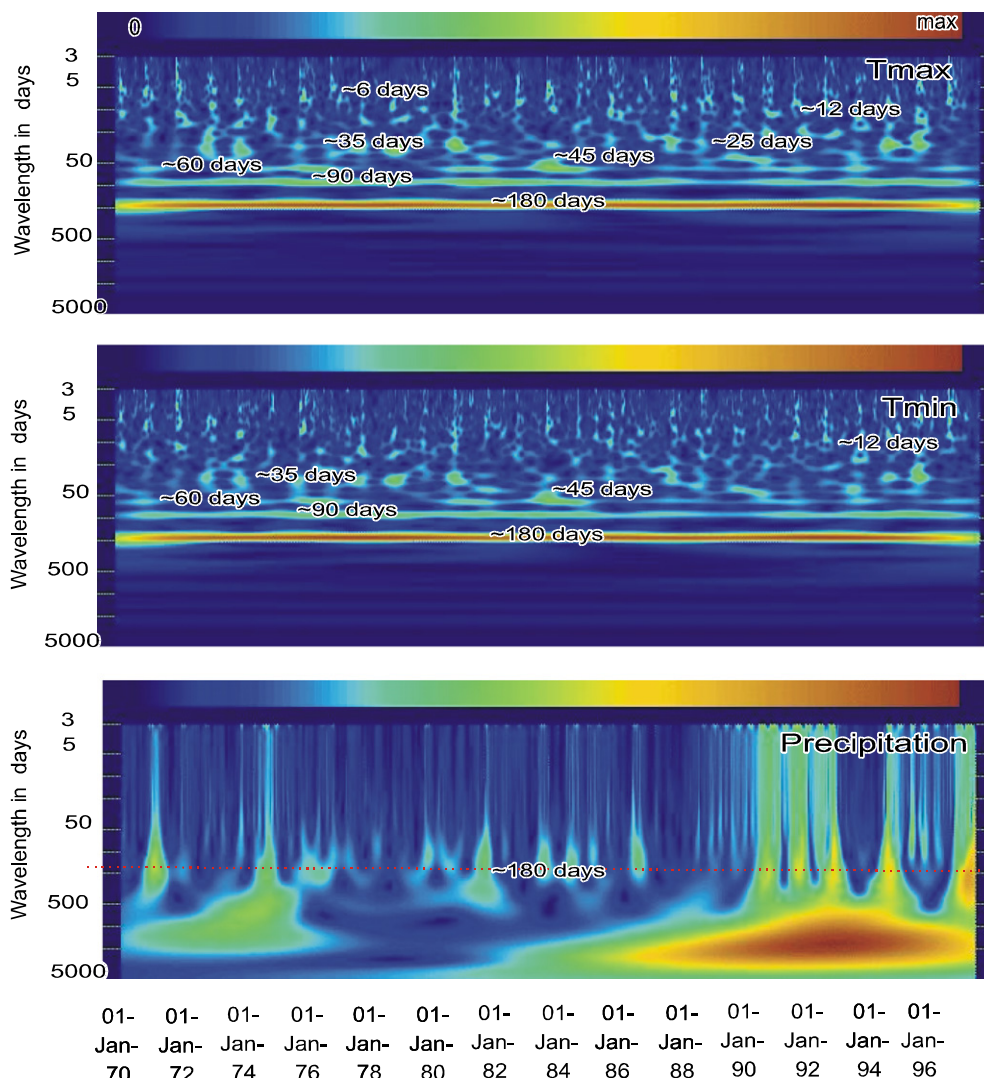


Figure 3 Overview wavelet analysis of Rideau River meteorological-training data.

Narrowband wavelet analysis

Narrowband wavelet decomposition analysis was used to decompose the six most important wavebands (i.e. 5–7 days, 10–15 days, 22–28 days, 30–35 days, 44–52 days, and 180–183 days) into their exact wavelengths with their amplitudes and phase. This step was done on the six wavebands (i.e. 5–7 days to 180–183 days) for all variables (i.e. F , P , TI , and TA). The averaged results of narrowband wavelet analysis in terms of the average amplitude and wavelength for each Julian day of each year of the training data for each waveband/signal can be found in Tables 5 and 6, respectively. The phase for each component at $t = 1$ can be found in Table 8.

Narrowband wavelet scalograms and phase spectrum figures

From the narrowband wavelet scalogram of the F data in Fig. 2, one can see the strength of the six chosen wavebands (i.e. ~ 6 days, ~ 12 days, ~ 25 days, ~ 35 days, ~ 45 days, and ~ 180 days). Horizontal lines indicate stationarity while

'speckled' data indicate non-stationarity. The long horizontal yellow/orange line around the 180 day scale in the scalogram indicates that the annual signal is stationary.

Comparative analysis of the four forecasting methods for 1 day lead-time

Table 12 shows the results of the best model of each method for 1 day lead-time forecasting. For comparative purposes, the 'perseverance model' (PM (1)) result is also shown in Table 12. The results show that highly accurate forecast values can be obtained from all four different methods with a lead-time of one day.

The following are the best four models that were developed from the four methods to forecast the stream flow in the Rideau River for 1 day lead-time:

- (1) The best regression model is MLR (1)-1, which had the lowest RMSE values of 17.9013 and 17.8034 in training and testing respectively, the highest R^2 values of 0.9476 and 0.9481 in training and testing respectively, and the highest testing EI value of 0.9480.

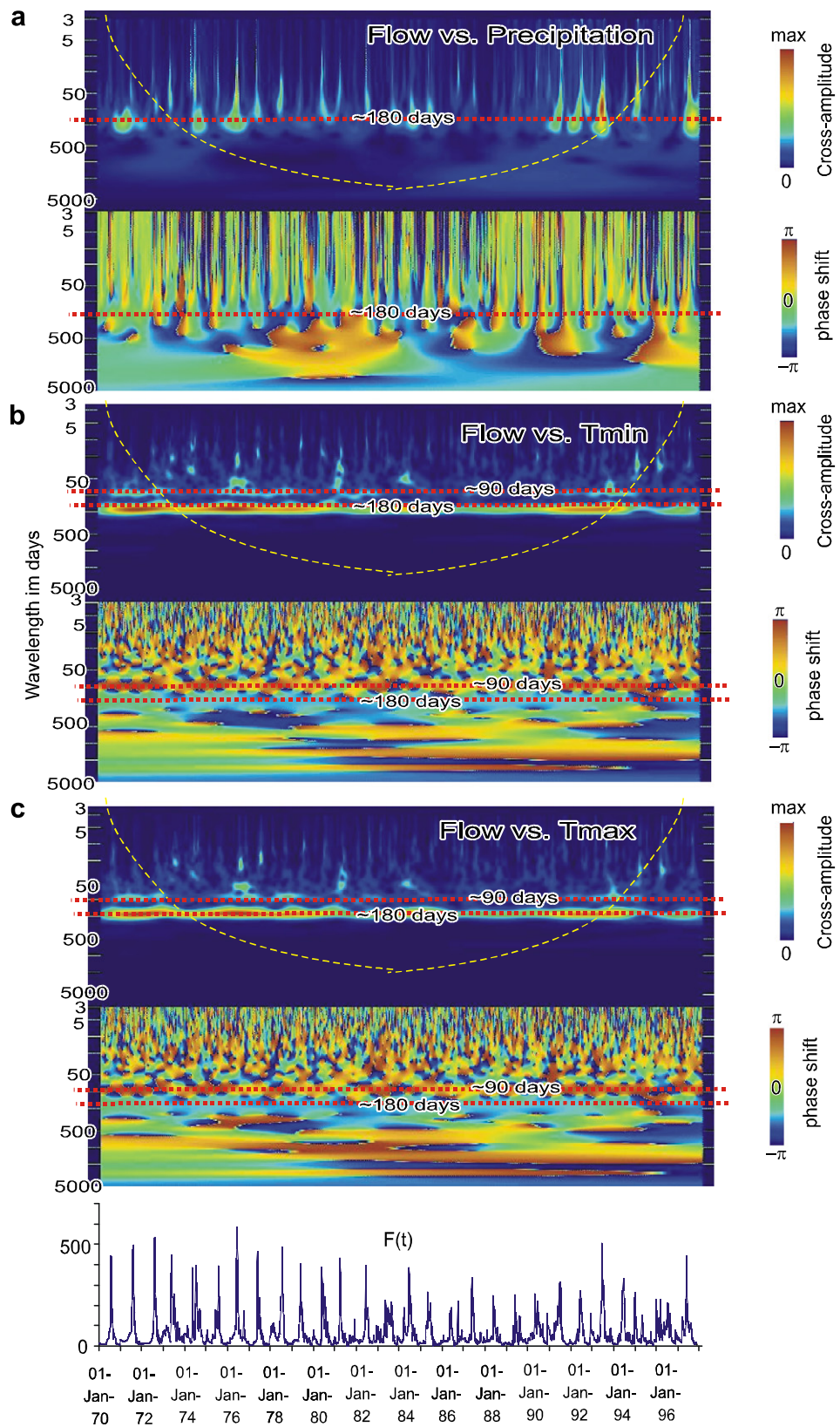
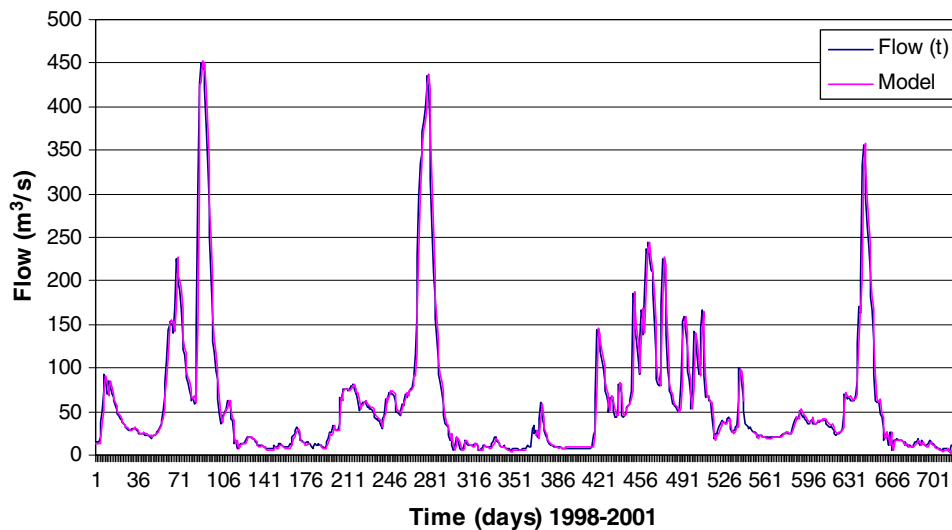


Figure 4 Cross-wavelet analysis of Rideau River training data top halves = wavelet coefficients; bottom halves = phase shift; x-axis = time in days, y-axis = wavelength in days; bottom of figure = $F(t)$ of training data.

Table 12 Performance statistics for best models for each method for 1 day lead-time

Model	RMSE training	RMSE testing	R^2 training	R^2 testing	EI testing
PM (1)	17.6847	17.4168	0.9493	0.9504	0.9486
MLR (1)-1	17.9013	17.8034	0.9476	0.9481	0.9480
ARIMA (1)-(3,1,0)	13.4309	13.9503	0.9674	0.9648	0.9631
ANN (1)-1	16.1034	16.1233	0.9496	0.9495	0.9492
WT (1)-M12	13.3370	13.8229	0.9778	0.9753	0.9744

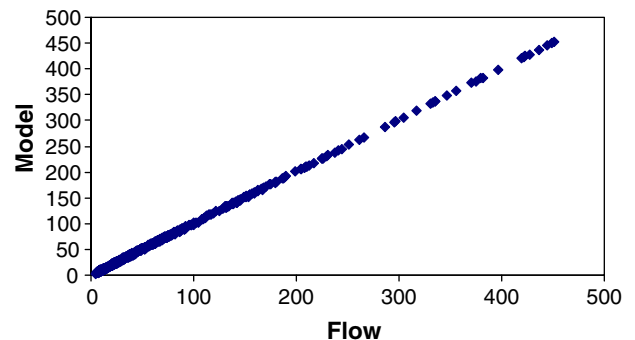
**Figure 5** Best Rideau River WT model for 1 day lead-time (WT(1)-M12).

- (2) The best ARIMA model is ARIMA (1)-(3,1,0), which had the lowest RMSE values of 13.4309 and 13.9503 in training and testing respectively, the highest R^2 values of 0.9674 and 0.9648 in training and testing respectively, and the highest testing EI value of 0.9631.
- (3) The best ANN model is ANN (1)-1, which had the lowest RMSE values of 16.1034 and 16.1233 in training and testing respectively, the highest R^2 values of 0.9496 and 0.9495 in training and testing respectively, and the highest testing EI value of 0.9492.
- (4) The best wavelet model is WT (1)-M12 which had the lowest RMSE values of 13.3370 and 13.8229 in training and testing respectively, the highest R^2 values of 0.9778 and 0.9753 for training and testing respectively, and the highest testing EI value of 0.9744.

Overall, the best forecasting model for 1 day lead-time was a wavelet analysis model. Model WT (1)-M12 had the highest testing R^2 , the lowest testing RMSE, and the highest testing EI of all models developed for 1 day lead-time forecasting. WT (1)-M12 had a testing RMSE that was 0.92% more accurate than ARIMA (1)-(3,1,0) (the best non-WT model), and a testing RMSE that was 26% more accurate than the 1 day perseverance model PM (1). WT (1)-M12 had a testing R^2 that was 1.1% more accurate than ARIMA (1)-(3,1,0), and a testing R^2 that was 2.55% more accurate than the 1 day perseverance model. And finally, WT (1)-M12 had a testing EI that was 1.2% more accurate than ARIMA (1)-(3,1,0),

and a testing EI that was 2.65% more accurate than the 1 day perseverance model.

Fig. 5 compares the observed and forecasted flow from model WT (1)-M12. Medium flows and high flows were very accurately forecasted, with low flows being somewhat less accurate. However, overall, it can be seen that the wavelet model forecasts low, medium, and high Rideau River flows very well for a lead-time of 1 day. Fig. 6 shows the scatter plot of observed and forecasted flow from model WT (1)-M12. It indicates a strong positive correlation.

**Figure 6** Scatter plot of best WT model for 1 day lead-time (WT(1)-M12).

It can be seen that the proposed stand-alone wavelet forecasting method is highly accurate for 1 day lead-time flood forecasting, and performs better than the MLR, ARIMA, and ANN methods.

Comparative analysis of the four forecasting methods for 2 days lead-time

As expected, when the lead-time increased from 1 day to 2 days, the performance of all the models decreased and less accurate forecast values were obtained. Table 13 shows the results of the best model of each method for 2 days lead-time forecasting. For comparative purposes, the 'perseverance model' (PM (2)) result is also shown in Table 13. The following are the best four models which were developed from the four methods to forecast the stream flow in the Rideau River for 2 days lead-time:

- (1) The best regression model is MLR (2) - 1 which had the lowest RMSE values of 36.8036 and 36.9167 in training and testing respectively, the highest R^2 values of 0.7859 and 0.7795 in training and testing respectively, and the highest testing EI value of 0.7792.
- (2) The best ARIMA model is ARIMA (2)-(3,1,0) which had the lowest RMSE values of 60.0341 and 65.8156 in training and testing respectively, the highest R^2 values of 0.7187 and 0.6576 in training and testing respectively, and the highest testing EI value of 0.3067.

- (3) The best ANN model is ANN (2)-4 which had the lowest RMSE values of 31.7062 and 31.9987 in training and testing respectively, the highest R^2 values of 0.8285 and 0.8236 in training and testing respectively, and the highest testing EI value of 0.8211.
- (4) The best wavelet model is WT (2)-M12, which had the lowest RMSE values of 31.0323 and 31.7985 in training and testing respectively, the highest R^2 values of 0.8477 and 0.8461 for training and testing respectively, and the second highest testing EI value of 0.8410.

Overall, the best forecasting model for 2 days lead-time was a wavelet model. Model WT (2)-M12 had the highest testing EI, the lowest testing RMSE, and the highest testing R^2 . WT (2)-M12 had a testing RMSE that was 0.63% more accurate than ANN (2)-4 (the best non-WT model), and a testing RMSE that was 32% more accurate than the 2 day perseverance model PM (2). WT (2)-M12 had a testing R^2 that was 2.66% more accurate than ANN (2)-4, and a testing R^2 that was 14.4% more accurate than the 2 day perseverance model. And finally, WT (2)-M12 had a testing EI that was 2.36% more accurate than ANN (2)-4, and a testing EI that was 13.7% more accurate than the 2 day perseverance model.

Fig. 7 compares the observed and forecasted flow using model WT (2)-M12. It can be seen that the stream flows were very slightly overestimated during high flow periods

Table 13 Performance statistics for best models for each method for 2 days lead-time

Model	RMSE training	RMSE testing	R^2 training	R^2 testing	EI testing
PM (2)	41.2925	41.9870	0.7394	0.7298	0.7199
MLR (2)-1	36.8036	36.9167	0.7859	0.7795	0.7792
ARIMA (2)-(3,1,0)	60.0341	65.8156	0.7187	0.6576	0.3067
ANN (2)-4	31.7062	31.9987	0.8285	0.8236	0.8211
WT (2)-M12	31.0323	31.7985	0.8477	0.8461	0.8410

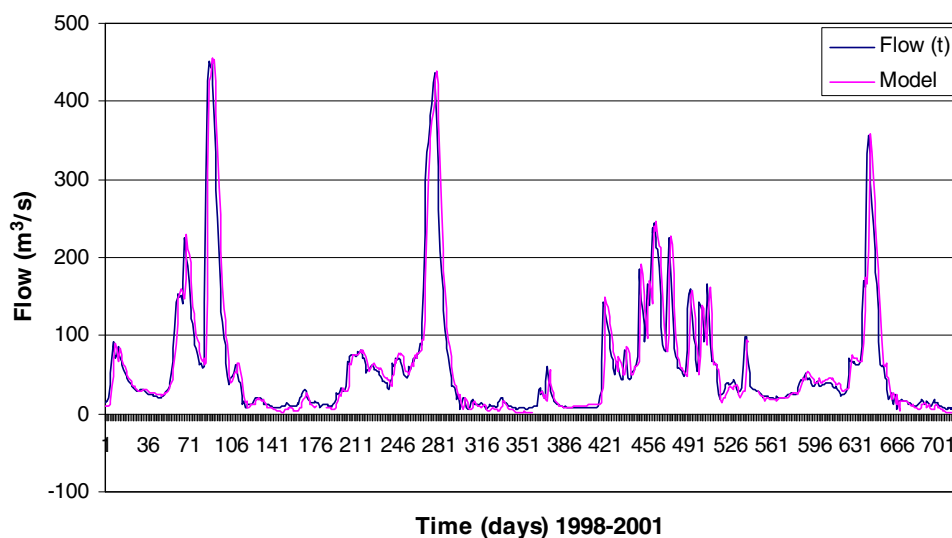


Figure 7 Best Rideau River WT model for 2 days lead-time (WT(2)-M12).

and both slightly overestimated and underestimated at different times during low flow periods. As well, a shift to the right in the forecasted flow can be observed. Fig. 8 shows the scatter plot of observed and forecasted flow from model WT (2)-M12. It indicates a relatively strong and positive correlation.

Overall, it can be seen that the proposed stand-alone wavelet forecasting method is highly accurate for 2 days lead-time flood forecasting, and performs better than the MLR, ARIMA, and ANN methods.

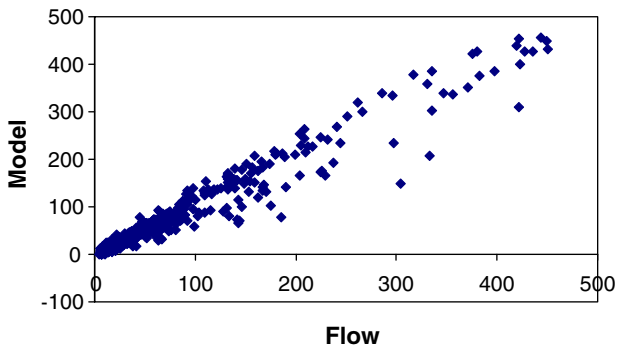


Figure 8 Scatter plot of best WT model for 2 days lead-time (WT(2)-M12).

Comparative analysis of the four forecasting methods for 6 days lead-time

The results show that as the lead-time increased the performance of all the models decreased and less accurate forecast values were obtained for each of the four different methods. Table 14 shows the results of the best model of each method for 6 days lead-time forecasting. For comparative purposes, the ‘perseverance model’ (PM (6)) result is also shown in Table 14. The following are the best four models which were developed from the four methods to forecast the stream flow in the Rideau River for 6 days lead-time:

- (1) The best regression model is MLR (6)-1 which had the lowest RMSE values of 59.0125 and 62.1031 in training and testing respectively, the highest R^2 values of 0.4294 and 0.3792 in training and testing respectively, and the highest testing EI value of 0.3781.
- (2) The best ARIMA model is ARIMA (6)-(3,1,0) which had the lowest RMSE values of 90.1039 and 97.7038 in training and testing respectively, the highest R^2 values of 0.3487 and 0.2378 in training and testing, respectively, and the highest testing EI value of -0.5405.
- (3) The best ANN model is ANN (6)-1 which had the lowest RMSE values of 50.0116 and 52.9023 in training and testing respectively, the highest R^2 values of 0.5891 and 0.5485 in training and testing respectively, and the highest testing EI value of 0.5476.

Table 14 Performance statistics for best models for each method for 6 days lead-time

Model	RMSE training	RMSE testing	R^2 training	R^2 testing	EI testing
PM (6)	68.4212	73.0954	0.3789	0.3143	0.2314
MLR (6)-1	59.0125	62.1031	0.4294	0.3792	0.3781
ARIMA (6)-(3,1,0)	90.1039	97.7038	0.3487	0.2378	-0.5405
ANN (6)-1	50.0116	52.9023	0.5891	0.5485	0.5476
WT (6)-M12	54.1691	57.6917	0.5391	0.4835	0.4366

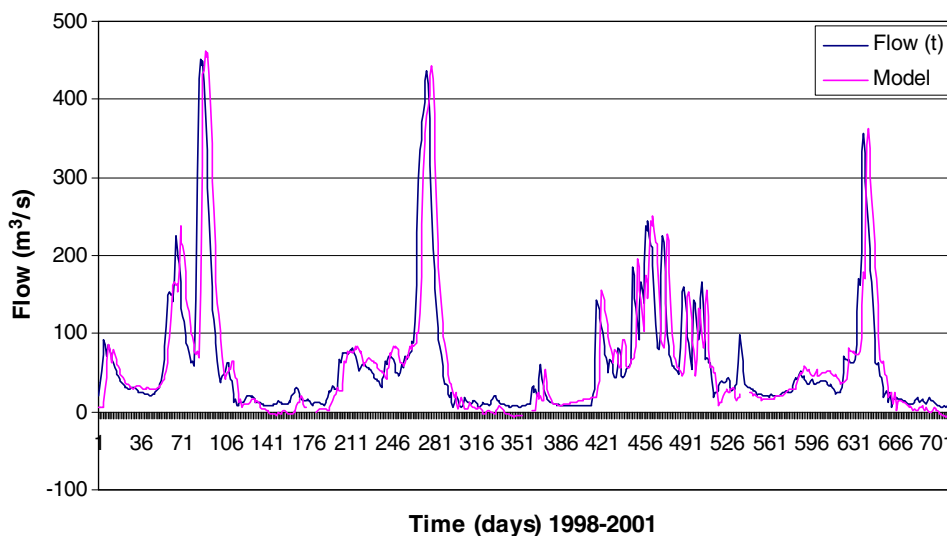


Figure 9 Best Rideau River WT model for 6 days lead-time (WT(6)-M12).

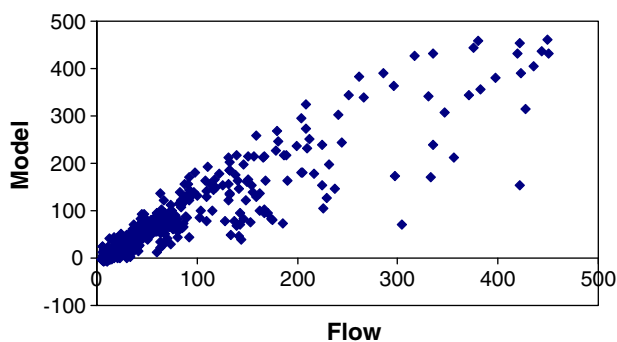


Figure 10 Scatter plot of best WT model for 6 days lead-time (WT(6)-M12).

- (4) The best wavelet model is WT (6)-M12 which had the lowest RMSE values of 54.1691 and 57.6917 in training and testing respectively, the highest R^2 values of 0.5391 and 0.4835 for training and testing respectively, and the second highest testing EI value of 0.4366.

Overall, the best forecasting model for 6 days lead-time is an ANN model. Model ANN (6)-1 had the lowest testing RMSE, the highest testing EI, and the highest testing R^2 . It was found that the wavelet analysis method is not as suitable for longer lead-time flood forecasting such as 6 days, and that the ANN method clearly provides more accurate results. ANN (6)-1 (the best overall model) had a testing RMSE that was 9.1% more accurate than WT (6) - M12 (the best wavelet model), although WT (6)-M12 still had a testing RMSE that was 26.7% more accurate than the 6 day perseverance model PM (6). ANN (6)-1 had a testing R^2 that was 11.8% more accurate than WT (6)-M12, although WT (6)-M12 still had a testing R^2 that was 35% more accurate than the 6 day perseverance model. And finally, ANN (6)-1 had a testing EI that was 20.3% more accurate than WT (6)-M12, although WT (6)-M12 still had a testing EI that was 47% more accurate than the 6 day perseverance model.

Fig. 9 compares the observed and forecasted flow using model WT (6)-M12. It can be seen that the stream flows were underestimated during low flow periods, and overestimated during medium and high flow periods. As well, a noticeable shift to the right in the forecasted flow can be observed. Fig. 10 shows the scatter plot of observed and forecasted flow from model WT (6)-M12. It indicates a weak positive correlation.

Overall, it can be seen that the proposed stand-alone wavelet forecasting method is more accurate for 6 days lead-time flood forecasting than the MLR and ARIMA methods, however, it is less accurate than the ANN method. As such, the results of this study indicate that the ANN method is more useful for 'longer-term' flood forecasting than the proposed WT method.

Discussion

Best model

The best wavelet model for the Rideau River for 1, 2, and 6 days lead-time forecasting was 'model M12' which can be

described, for example in the case of 2 days lead-time forecasting, by

$$F(t-3) + [TI182(t) - TI182(t-3)] + [F48(t) - F48(t-3)] \\ + [TA12(t) - TA12(t-3)] + [P5(t) - P5(t-3)] + [F25(t) \\ - F25(t-3)]$$

This model is a 'mixed' variable and signal model. It can be seen that in the case of the Rideau River, the changes in cyclical outputs of all four variables (i.e. F , P , TI , and TA) with varying wavelengths (i.e. 182, 48, 25, 12, and 5 days) provided the most accurate forecasting model. More specifically, it was found that the ~ 182 day minimum temperature cycles ($TI182$), the ~ 48 day flow cycles ($F48$), the ~ 25 day flow cycles ($F25$), the ~ 12 day maximum temperature cycles ($TA12$), and the ~ 5 day precipitation cycles ($P5$), provided the most accurate forecasting models for 1, 2, and 6 days flood forecasting. Apart from this, it is difficult to provide any additional physical insight on the final form of the wavelet models.

Strength of the dominant annual signal

The dominant annual signal was found to be the most useful constituent component in the forecasting models for each of the three lead-times. The reason for this is that the 182 day cycle was very well-defined, most likely because of the continental climate setting of Ottawa, and because the wavelength (or onset–offset in each year) was very stable for the annual cycle. The dominant annual signal was the only signal that was found to be stationary. All other signals were non-stationary. The occurrences of the shorter cycles were less stable (for example the phases were less stable). Nevertheless, the use of shorter cycles in combination with the annual cycle proved to be advantageous.

High accuracy of 1 and 2 days lead-time and low accuracy of 6 days lead-time forecasting with wavelet models

A possible reason for the excellent performance of the 1 and 2 days lead-time wavelet forecasting models could be the relationship between one of the defining properties of the short-term wavelet based forecasting procedure (i.e. local daily non-stationarity of the forecast model) and the same property of the real river flood flow process. Recent research by Wang (2006) has shown that the shorter the lead-time, the more likely a hydrological process is non-linear and non-stationary. More specifically, Wang states that almost all yearly hydrological processes are linear and stationary while at the other end almost all daily river flood flow processes are non-linear and non-stationary. As such, it is likely that the property of local daily non-stationarity that is a defining characteristic of the wavelet method is very useful and allows for more precise forecasting.

It was found that the wavelet model for 6 days lead-time forecasting was not particularly accurate, with the best ANN model being more accurate. It was difficult to find any 'technical' or physical reason as to why the 6 days lead-time

wavelet model was not very accurate. It is likely that the averaging that is necessary for the wavelet model affects the longer forecasts to a greater degree. It could also be that the ANN method is simply better suited for longer forecasting lead-times.

Artificially splitting the training data

In order to obtain the best possible forecasting models, one must carefully consider the following two issues: (a) split the data artificially so that the constituent components only deal with the period of interest for forecasting, but have potentially significant edge effect problems and possibly phase problems; or (b) not split the data artificially so that the constituent components deal with the entire year and as such not have potentially significant edge effect or phase problems, but have unwanted remains of influences of cycles from the period of the year not being forecasted.

It was found that it is very difficult to decide *a priori* (before analysis/modeling starts) if the artificial splitting of the data would have a large or small effect on particular wavebands and variables. In order to determine whether it is advisable to artificially split the data, it is necessary to analyze the split data in great detail. For example, if the causes of floods are completely different at certain points of the year (which was the case for the Rideau River), artificially splitting the data for those specific periods should be considered. Wavelet based forecasting models can then be developed specifically for those periods, as in the Rideau River case.

In future studies, if it is decided to artificially split the data, then an 'edge effect correction for split data' such as the one developed in this study, should be applied. As well, a value of $l = 5$ is recommended in the wavelet and cross-wavelet decomposition stages for any future studies since, during the experimental stages of this study, it was found that such a value significantly 'dampens' the effect of amplitude and phase jumps carried into the new analyzing window each year when using artificially split data. Without the use of the edge effect correction technique developed in this study, along with the use of $l = 5$ for 'dampening', it might be difficult to effectively use artificially split data in the development of wavelet based constituent components for flood forecasting.

Conclusion

There are a number of issues with respect to the use of wavelet and cross-wavelet analysis for flood forecasting snowmelt driven floods within the areas of water resources engineering and hydrology that were explored in this study that, to the best knowledge of the author, have not been explored in any great detail in the literature. The main conclusions of this research are

1. The use of wavelet analysis in the development of a stand-alone wavelet based short-term river flood forecasting method was shown to be useful for 1 and 2 day lead-time forecasting, assuming that there are no *significant* trends in the amplitude for the same Julian day
2. The use of cross-wavelet analysis in the development of short-term river flood forecasting models was shown to be useful, assuming there is a relatively stable phase shift between the flow and meteorological time series. Cross-wavelet analysis was used to find phase differences between flow and meteorological data and to develop cross-wavelet constituent components, both of which improved the forecasting ability of the wavelet based flood forecasting models.
3. The use of wavelet decomposed meteorological data, in addition to wavelet decomposed flow data, was shown to be useful in the development of models for short-term river flood forecasting. In order to be able to use the wavelet decomposed meteorological data for flood forecasting, a calibration constant was developed in this study and its usefulness was demonstrated in linking specific wavelengths of flow and meteorological cycles.
4. The use of an edge effect correction technique developed from the continuous wavelet transform for artificially split flow and meteorological data, was shown to be useful in applications where data are split artificially. In order to account for significant edge effect discontinuities resulting from artificial amplitude jumps due to artificial splitting of data, an edge effect correction technique was developed in this study, and its usefulness was demonstrated.
5. The use of a modified version of the inverse Fourier transform with a calibration constant and an edge effect correction for short-term river flood forecasting was shown to be useful for the reconstruction of wavelet and cross wavelet derived constituent components. In order to reconstruct wavelet decomposed signals, the inverse Fourier transform can be used. However, in order to allow for a more precise reconstruction, an edge effect correction and a calibration constant for meteorological signals was applied to the inverse Fourier transform in this study.

The development of a stand-alone data-based flood forecasting method based on wavelet and cross-wavelet analysis, with the above mentioned original contributions not found in the literature, was the main contribution of this research.

There are several recommendations for future research that can be made based on the results of this research:

1. It would be very useful to develop a new 'flood mother wavelet' that is based partially on the Morlet mother wavelet in order to assess its usefulness specifically for flood forecasting applications. Two possible improvements that could be made to the Morlet mother wavelet for specific use in flood forecasting applications include: (1) extending the Gaussian envelope of the Morlet mother wavelet so that the peaks and troughs extend further in the vertical direction and (2) modifying the peaks and troughs of the Morlet wavelet so that they

are more 'spiky'. It is possible that this modified Morlet wavelet or 'flood mother wavelet' could allow for more precise wavelet decomposition, which would increase the forecasting ability of the wavelet based constituent components.

2. It would be very useful to explore the use of the proposed wavelet based flood forecasting method developed in this study in applications where there is a significant trend in the amplitude for the same Julian day year-to-year. In such cases, the actual forecasting component of the proposed method could be modified to take into account any significant trend.
3. It would be useful to test the use of upstream streamflow and meteorological inputs, and radar, radiosonde, and satellite data, as well as real time updating mechanisms such as error prediction, state updating, and parameter updating in conjunction with the proposed wavelet based forecasting method. Such 'additions' would most likely improve the accuracy of the flood forecasts obtained using the proposed wavelet based method.

To summarize, two main conclusions can be derived from the results of this study:

1. It was found that the proposed wavelet based flood forecasting method can be successfully applied as a highly accurate stand-alone method for short-term 1 and 2 days lead-time flood forecasting.
2. In the case of 6 days lead-time flood forecasting, the newly developed wavelet based forecasting method was found to be less accurate than the ANN method. This indicates that the proposed wavelet based flood forecasting method is less suitable for longer lead-times such as 6 days.

Acknowledgements

The author would like to thank his supervisor Professor Janusz Kindler of the Institute of Environmental Engineering Systems at the Warsaw University of Technology for his very valuable advice throughout the course of this research. As well, comments provided by Professor Marek Nawalany of the Institute of Environmental Engineering Systems at the Warsaw University of Technology, and Professor Jaroslaw Napiorkowski of the Institute of Geophysics at the Polish Academy of Sciences, are also appreciated.

References

- Appenzeller, C., Stocker, T.F., Anklin, M., 1998. North Atlantic oscillation dynamics recorded in Greenland ice cores. *Science* 282, 446–449.
- Aussem, A., Campbell, J., Murtagh, F., 1998. Wavelet-based feature extraction and decomposition strategies for financial forecasting. *Journal of Computational Intelligence in Finance* 6, 5–12.
- Aussem, A., Murtagh, F., 1997. Combining neural network forecasts on wavelet transformed time series. *Connection Science* 9, 113–121.
- Baliunas, S., Frick, P., Sokoloff, D., Soon, W., 1997. Time scales and trends in the Central England temperature data (1659–1990) – a wavelet analysis. *Geophysical Research Letters* 24, 1351–1354.
- Cannas, B., Fanni, A., Sias, G., Tronei, S., Zedda, M.K., 2005. River flow forecasting using neural networks and wavelet analysis. In: EGU 2005, European Geosciences Union, Vienna, Austria, 24–29 April, 2005.
- Coulibaly, P., Anctil, F., Bobee, B., 2000. Daily reservoir inflow forecasting using artificial neural networks with stopped training approach. *Journal of Hydrology* 230, 244–257.
- Curry, K., Bras, R.L., 1980. *Multivariate Seasonal Time Series Forecast with Application to Adaptive Control*. MIT Technical Publication.
- Gamage, N., Blumen, W., 1993. Comparative analysis of low level cold fronts: wavelet, Fourier, and empirical orthogonal function decompositions. *Monthly Weather Review* 121, 2867–2878.
- Gedalof, Z., Smith, D.J., 2001. Interdecadal climate variability and regime-scale shifts in Pacific North America. *Geophysical Research Letters* 28, 1515–1518.
- Grossman, A., Morlet, J., 1984. Decomposition of Hardy functions into square integrable wavelets of constant shape. *SIAM Journal on Mathematical Analysis* 15, 723–736.
- Gu, D., Philander, S.G., 1995. Secular changes of annual and interannual variability in the tropics during the past century. *Journal of Climate* 8, 864–876.
- Hsu, K., Gupta, H.V., Gao, X., Sorooshian, S., Imam, B., 2002. Self-organizing linear output map (SOLO): an artificial neural network suitable for hydrologic modeling and analysis. *Water Resources Research* 38, 3810–3817.
- Hsu, K., Gupta, H.V., Sorooshian, S., 1995. Artificial neural network modelling of rainfall–runoff process. *Water Resources Research* 31, 2517–2530.
- Hudgins, L., Friehe, C.A., Mayer, M.E., 1993. Wavelet transforms and atmospheric turbulence. *APS Physical Review* 71, 3279–3282.
- Ikeda, M., Tokinaga, S., 1999. A prediction method for stock prices. *Journal of the Operations Research Society of Japan* 40, 18–31.
- Jury, M.R., Enfield, D.B., Melice, J.L., 2002. Tropical monsoons around Africa: stability of El Nino-southern oscillation associations and links with continental climate. *Journal of Geophysical Research*, 107.
- Kang, K.W., Kim, J.H., Park, C.Y., Ham, K.J., 1993. Evaluation of hydrological forecasting system based on neural network model. In: *Proceedings of the 25th Congress of the International Association for Hydraulic Research*, Delft, Netherlands, pp. 257–264.
- Kim, G., Barros, A.P., 2001. Quantitative flood forecasting using multisensor data and neural networks. *Journal of Hydrology* 246, 45–62.
- Kim, T.W., Valdes, J.B., 2003. A nonlinear model for drought forecasting based on conjunction of wavelet transforms and neural networks. *Journal of Hydrologic Engineering* 8, 319–328.
- Labat, D., Ababou, R., Mangin, A., 1999. Wavelet analysis in Karstic hydrology 2nd Part: rainfall–runoff cross-wavelet analysis. *Comptes Rendus de l'Academie des Sciences Series IIA Earth and Planetary Science* 329, 881–887.
- McKerchar, A.I., Delleur, J.W., 1974. Application of seasonal parametric linear stochastic models to monthly flow data. *Water Resources Research* 10, 246–255.
- Morlet, J., Arens, G., Fargeau, I., Giard, D., 1982. Wave propagation and sampling theory. *Geophysics* 47, 203–236.
- Nash, J.E., Sutcliffe, J.V., 1970. River flow forecasting through conceptual models Part I: a discussion of principles. *Journal of Hydrology* 10, 282–290.
- Nayak, P.C., Sudheer, K.P., Rangan, D.M., Ramasastni, K.S., 2005. Short-term flood forecasting with a neurofuzzy model. *Water Resources Research* 41, 1–16.

- Noakes, D.J., McLeod, A.I., Hipel, K.W., 1985. Forecasting monthly riverflow time series. *International Journal of Forecasting* 1, 179–190.
- Phien, H.N., Huong, B.K., Loi, P.D., 1990. Daily flow forecasting with regression analysis. *Water SA* 16, 179–184.
- Piotrowski, A., Napiorkowski, J.J., Rowinski, P.M., 2006. Flash-flood forecasting by means of neural networks and nearest neighbour approach – a comparative study. *Nonlinear Processes in Geophysics* 13, 443–448.
- Prokoph, A., 2006. XCWT.F cross-wavelet software program. Unpublished.
- Prokoph, A., Barthelmes, F., 1996. Detection of nonstationarities in geological time series: wavelet transform of chaotic and cyclic sequences. *Computers and Geosciences* 10, 1097–1108.
- Saco, P., Kumar, P., 2000. Coherent modes in multiscale variability of streamflow over the United States. *Water Resources Research* 36, 1049–1068.
- Smith, L.C., Turcotte, D.L., Isacks, B.L., 1998. Stream flow characterization and feature detection using a discrete wavelet transform. *Hydrological Processes* 12, 233–249.
- Soltani, S., Boichu, D., Simard, P., Canu, S., 2000. The long-term memory prediction by multiscale decomposition. *Signal Processing* 80, 2195–2205.
- Tangborn, W.V., Rasmussen, L.A., 1976. Hydrology of the North Cascades region, Washington – Part 2: a proposed hydrometeorological streamflow prediction method. *Water Resources Research* 12, 203–216.
- Tantane, S., Patamatammakul, S., Oki, T., Sriboonlue, V., Prempree, T., 2005. Coupled wavelet-autoregressive model for annual rainfall prediction. *Journal of Environmental Hydrology*, 13.
- Tawfik, M., 2003. Linearity versus non-linearity in forecasting Nile River flows. *Advances in Engineering Software* 34, 515–524.
- Tolland, L., Cathcart, J.G., Russell, S.O.D., 1998. Estimating the Q100 in British Columbia: a practical problem in forest hydrology. *Journal of the American Water Resources Association* 34, 787–794.
- Torrence, C., Compo, G., 1998. A practical guide to wavelet analysis. *Bulletin of the American Meteorological Society* 79, 61–78.
- Wang, R., Lee, T., 1998. A study on the wavelet model of upland watersheds and its application to hydrological estimation. *Proceedings of Statistical Methods for Hydrologic Systems* 31 (August), 12–21.
- Wang, W., 2006. Stochasticity, nonlinearity and forecasting of streamflow processes. PhD Thesis. Delft University.
- Wong, H., Ip, C., Xie, Z.J., Lui, X.L., 2003. Modelling and forecasting by wavelets and the application to exchange rates. *Journal of Applied Statistics* 30, 537–553.
- Yurekli, K., Kurung, A., Ozturk, F., 2005. Testing the residuals of an ARIMA model on the Cekerek stream watershed in Turkey. *Turkish Journal of Engineering and Environmental Sciences* 29, 61–74.
- Zhang, B.L., Dong, Z.Y., 2001. An adaptive neural-wavelet model for short term load forecasting. *Electric Power Systems Research* 59, 121–129.
- Zheng, T., Girgis, A.A., Makram, E.B., 2000. A hybrid wavelet-Kalman filter method for load forecasting. *Electric Power Systems Research* 54, 11–17.